Hindawi
Shock and Vibration
Volume 2020, Article ID 5731721, 16 pages
https://doi.org/10.1155/2020/5731721

Research Article

Study on Failure Modes and Energy Evolution of Coal-Rock Combination under Cyclic Loading

Shilin Song,[1] Xuesheng Liu,[1,2] Yunliang Tan,[1] Deyuan Fan,[1] Qing Ma,[1] and Honglei Wang[1]

[1]*State Key Laboratory of Mining Disaster Prevention and Control Co-Founded by Shandong Province and the Ministry of Science and Technology, Shandong University of Science and Technology, Qingdao 266590, China*
[2]*State Key Laboratory of Water Resource Protection and Utilization in Coal Mining, China Energy Group Co., Ltd., Beijing 100011, China*

Correspondence should be addressed to Xuesheng Liu; xuesheng1134@163.com

Received 30 August 2019; Accepted 6 November 2019; Published 20 January 2020

Academic Editor: Salvatore Russo

The loading modes and roof lithology have a significant influence on the mechanical properties of coal seams. To reveal the failure modes and energy evolution law of underground coal during the mining process, conventional uniaxial and uniaxial cyclic loading tests were carried out on three types of samples: coal, rock, and coal-rock combinations. The results show that the samples mainly behave with three failure modes (shear slip, tensile splitting, and fracture), and all the coal sections in the coal-rock combinations fail, whereas most rock sections remain intact. The compressive strength of the coal-rock combination is higher than coal and much smaller than rock. Compared with the conventional uniaxial loading condition, both the maximum deformation before failure and Young's modulus under the cyclic loading condition are greater, and the latter increases quadratically with the cycle index. The energy densities are also calculated, and their variations are analysed in detail. The results show that with increasing cycle index, both the elastic energy stored in the sample and the dissipated energy increase in a quadratic function, and the failure process becomes more intense. This research reveals the failure modes, deformation characteristics, and energy evolution of the coal-rock combination under different loading conditions, which can provide strong support for controlling underground surrounding rocks of the coal face and roadway in coalmines.

1. Introduction

In the production process of an underground coal mine, production activities such as roadway excavation and coal face mining will cause strata movement and stress redistribution around the stope. Thus, a mining stress field is generated, and the stress changes continuously with mining activity [1–4]. Its superposition with the original rock stress acts on surrounding coal seams, the roof, and floor strata, which is a typical cyclic loading condition [5–7].

Scholars and engineers have carried out a significant amount of research on the law of deformation, failure, and energy evolution of coal and rock under cyclic loading. Compared with conventional uniaxial loading, Li et al. found that the fragments of coal and rock under cyclic loading are mostly irregular, wedge-shaped, and block-shaped, with obvious shape characteristics [8]. Xiao et al. found that with an increase in cycling index, the peak stress decreases, while the elastic energy and dissipated energy increase [9, 10]. Yang et al. carried out uniaxial cyclic loading tests on coal and rock. They found under cyclic loading, the destruction of samples is divided into three stages: the beginning stage, the stable deformation stage, and the accelerating deformation stage [11–13]. Yang et al. examined the mechanical damage characteristics of sandstone subjected to cyclic loading under triaxial compression condition. The result showed that the higher the unloading stress level, the more the work done on the coal and rock mass during

loading, the more the elastic energy released during unloading, and the greater the energy dissipation rate is, the shorter the fatigue life of coal sample (the proportion of dissipated energy to input energy) [14–16]. Deng et al. found that the confining pressure also has a significant influence on the energy evolution. The greater the confining pressure is, the greater the elastic strain energy accumulates in the rock, and more energy is consumed during the crack propagation process, meaning the energy dissipation increases [17–21].

In recent years, some scholars have realised that the coal seam and roof-and-floor rocks are loaded together in actual underground coal mine engineering. Hence, it is difficult to describe the instability of the whole structure by using the test results of single coal or rock sample. Therefore, the loading test of coal-rock combinations is presented, which is more consistent with the deformation and failure of an in situ coal seam and its surrounding rocks [22–24]. Chen et al. [25] studied the mechanical properties of coal-rock combinations with different height ratios and found that the uniaxial compressive strength and Young's modulus of the samples increased with increasing rock-coal height ratio. Moreover, most of the failures of the combination samples started from the coal section. Through uniaxial and triaxial loading tests of the coal-rock combination, Zhang et al. [26] obtained the deformation and failure characteristics under different combination modes. It was considered that the failure of these combinations mainly concentrated on the coal section, which had nothing to do with the combination and loading contact modes, and the failure of the coal section could induce the failure of the rock section to a certain extent. Through an in-depth analysis of the test results, Song et al. [27] established the postpeak nonlinear stress-strain relationship of coal-rock combinations and obtained the change trend in the postpeak stress-strain relationship. Zuo et al. [28] established the constitutive model of the crack body in the postpeak crack penetration stage by conceptualising the coal-rock combinations in the postpeak stage as a crack body and matrix. Zhu et al. [29] carried out uniaxial graded cyclic loading tests on coal-rock combinations. The results showed that shear failure was the main failure mode of coal-rock combinations, and the degree of damage was aggravated with the decrease in strength of the rock section. In summary, the existing studies obtained the basic mechanical properties and failure characteristics of coal-rock combinations by cyclic loading tests. However, there are few studies on the internal energy evolution of coal-rock combinations under cyclic loading, especially comparative studies on the energy evolution law with a single coal or rock sample. The energy evolution calculation method used in this study is proposed by Gong et al. and Tang et al. [30, 31]. Compared with the previous ones, this method can avoid the influence of hysteresis loop and the calculation result is more accurate and reliable.

By conducting conventional uniaxial and uniaxial cyclic loading tests on coal, rock, and coal-rock combinations, the deformation, strength, and failure characteristics of different samples were compared and analysed. Together with the calculation method of elastic energy and dissipated energy of a coal-rock combination under cyclic loading condition, the energy evolution law and its influential factors of the coal-rock combination were revealed. This could provide theoretical support for the stability control of the surrounding rocks of an underground coal roadway.

2. Experimental Setup

2.1. Specimen Preparation. The test samples included coal, mudstone, fine sandstone, and medium sandstone, which were taken from the 2-2 coal seam and its roof in Gaojialiang Coal Mine, Inner Mongolia. After the samples were ground, standard cylindrical samples with a diameter of 50 mm and lengths of 50 and 100 mm were prepared according to the method recommended by the International Society of Rock Mechanics. To reduce the discreteness of the test results caused by natural defects, samples with few cracks and no obvious defects were selected for testing. Further, the two ends of the samples were ground to avoid stress concentration during loading. Five samples with a height of 100 mm were processed, including two coal bodies, one mudstone, one fine sandstone, and one medium sandstone. In addition, 18 samples with a height of 50 mm were also processed, including 9 coal bodies, 3 mudstones, 3 fine sandstones, and 3 medium sandstones. After grinding, the coal and rock samples with a diameter of 50 mm and length of 50 mm were bonded together with 502-strong glue to make standard samples with a length of 100 mm. The coal samples, rock samples, and coal-rock combination samples used in the test are listed in Table 1, and the photographs of the samples are shown in Figure 1.

2.2. Experimental System. The loading system used in this test was an AG-X250 electronic universal testing machine manufactured by the Shimadzu Company of Japan. The test machine is composed of the host, loading test bed, and computer, as shown in Figure 2. It is driven by an AC servo motor. The loading mode adopts a double lead screw structure. The equipment has good stability and high precision, and the maximum test load is 250 kN. It has two loading control modes: the displacement control mode, in which the loading speed is 0.0005–1000 mm/min, and the stress control mode, in which the loading speed is 0.0001–10 kN/s. The machine is suitable for completing uniaxial compression, cyclic compression, and creep tests of rock, concrete, coal, and other materials.

When loading samples, strain gauges are used to monitor the strain of samples, and a DH3818N static strain tester is used to collect test data. The testing machine has its own pressure sensor, which can monitor the stress change of the sample during loading. The monitoring data are collected automatically by computer software, and they can be imported into Excel, Origin, and other data analysis software for processing and analysis.

2.3. Experimental Procedure. Two types of loading tests were carried out. One was the conventional uniaxial loading test of coal samples, rock samples, and coal-rock combination samples. The other was the uniaxial cyclic loading test of

Table 1: Samples used in this research.

Specimen type	Numbering	Height(mm)	Test method
Coal	M1-1	100.02	Conventional uniaxial loading test
	M1-2	100.05	
Mudstone	NY-1	100.09	
Mudstone-coal combination	NYM1-1	97.98	Uniaxial cyclic loading test
	NYM1-3	98.44	
	NYM1-4	100.11	
Fine sandstone	XS-1	100.02	Conventional uniaxial loading test
Fine sandstone-coal combination	XSM1-1	98.56	Uniaxial cyclic loading test
	XSM1-3	97.90	
	XSM1-4	100.16	
Medium sandstone	ZS-1	100.05	Conventional uniaxial loading test
Medium sandstone-coal combination	ZSM2-2	98.53	Uniaxial cyclic loading test
	ZSM2-6	98.68	
	ZSM2-7	100.14	

Figure 1: Samples for testing.

coal-rock combination samples. The specific test scheme is presented in Table 1.

Conventional uniaxial loading tests were carried out in accordance with the steps provided by the National Standard of China "methods for determining the uniaxial compressive strength and counting softening coefficient" (GB/T 23561.7–2009). In this experiment, the load control method was used to load the samples at a speed of 0.001 kN/s until they failed. The full stress-strain curves, uniaxial compressive strength, and Young's modulus of the samples were obtained. Conventional uniaxial loading tests were carried out eight times.

Based on the above test results, uniaxial cyclic loading tests of the coal-rock combinations were carried out. This experiment was carried out in accordance with the test method proposed in the national standard "classification and laboratory test method on bursting liability of coal-rock combination samples" (GB/T 25217.3) (draft). Some changes were made as follows: The loading speed of the testing machine was reduced from 1 to 0.001 kN/s, and the stress control mode was used, which was not changed during the test. The specific loading and unloading scheme was as follows: initial load $\longrightarrow$ 10% $\sigma_c \longrightarrow$ 0.5 kN $\longrightarrow$ 20% $\sigma_c \longrightarrow$ 0.5 kN $\longrightarrow$ 30% $\sigma_c \longrightarrow$ 40% $\sigma_c \longrightarrow$ 0.5 kN $\longrightarrow$ ... $\longrightarrow$ failure. The uniaxial cyclic loading tests were carried out nine times.

3. Results and Discussion

3.1. Macrofracture

3.1.1. Failure Modes. Identification of the failure modes of coal and rock samples plays an important role in underground

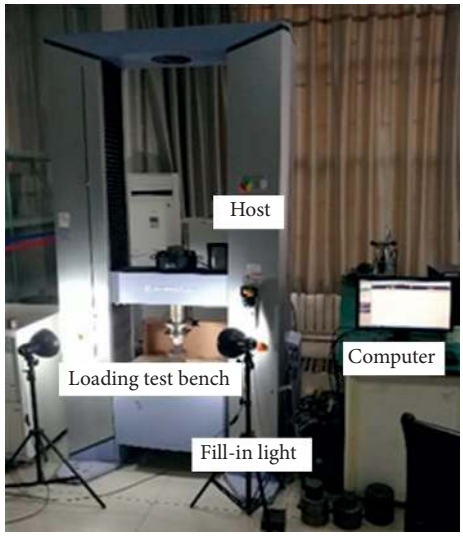

Figure 2: Shimadzu AG-X250 electronic universal testing machine.

excavation and supports the design of coal mines [32–37]. You and Hua [38] presented four failure modes of rock under uniaxial compression conditions: tension failure, penetrating shear failure, approximately conical tension failure, and fracture failure of rock fragments. Tang et al. [39] indicated that the failure modes of rock and soil in uniaxial and triaxial compression tests can be divided into five failure types: splitting, tension shear, shear, dilatancy, and bulging. Niu et al. [40] believed that the main failure mode of sandstone under uniaxial compression was splitting, and a few samples exhibited shear failure. In summary, the failure modes of samples under uniaxial compression can be approximately divided into three types of failure: shear slip, tensile splitting, and fracture. The failure modes are shown in Figure 3.

The failure modes of some samples are shown in Figure 4. It can be seen from the figure that the failure modes of these samples in the conventional uniaxial loading test were mostly fracture failure, with a large quantity of debris peeling off. A small number of samples had tension splitting failure with penetrating cracks. In the uniaxial cyclic loading test, the failure mode of most of the samples was similar to shear slip failure. There were large coal bodies caving out of the test bench. A small number of samples had penetrating cracks, and the failure of these samples was tensile splitting failure.

The results showed that the failure modes of coal and rock samples were mostly the typical fracture failure, and there was a large amount of debris spalling on one side of the samples, as shown in Figures 4(a)–4(c). There were also rock samples that exhibited typical tensile splitting failure and sudden failure in the test process, as shown in Figure 4(d). In the conventional uniaxial loading tests, the failure modes of the coal-rock combinations were also typical fracture failure, as shown in Figures 4(e) and 4(f). In the uniaxial cyclic loading tests, most of the samples exhibited typical shear slip failure. When the samples were destroyed, massive coal caved out of the test bench, as shown in Figures 4(g), 4(i)–4(l). In addition, there were coal-rock combinations in which the failure mode was tensile splitting failure, and the top rocks showed through the cracks, as shown in Figure 4(h).

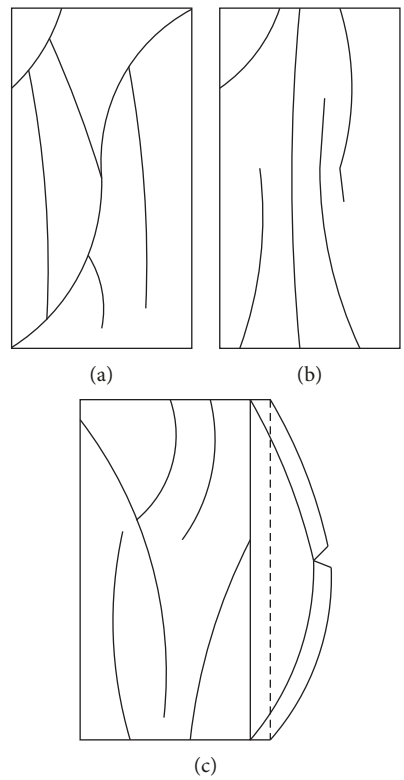

Figure 3: Failure modes of uniaxial compression. (a) Shear slip failure. (b) Tensile splitting failure. (c) Fracture failure.

In summary, from the perspective of failure mode, the failure modes of coal, rock, and coal-rock combination samples were the same in conventional uniaxial loading tests, and they belonged to the category of fracture failure. The failure of coal and rock samples turned into global failure, while the failure of coal-rock combination samples was mostly failure of the underlying coal body. This is due to the existence of the coal and rock interface in the combinations, and the transmission of force is affected. Because of the strength gap of the material itself, the failure of the coal body is prior to that of rock. In addition, in the uniaxial cyclic loading test, the failure modes of coal-rock combinations with different roof lithologies were different. If the roof lithology was weak, fracture failure easily occurred, but if the roof lithology was strong, shear slip failure occurred.

3.1.2. Deformation and Failure Characteristics. Coal and rock can be regarded as a heterogeneous multiphase composite structure with numerous natural defects, and the distribution of these defects is completely random. Under the action of external force, the microcracks inside the coal and rock body continuously sprout, expand, penetrate, and finally form macrofractures. The generation of macroscopic fractures leads to the instability of the coal and rock [41–43]. All the stress-strain curves have compaction, elastic deformation, yield, plastic failure, and postfracture stages, which correspond to different stages of the loading process. It is convenient to analyse the deformation and

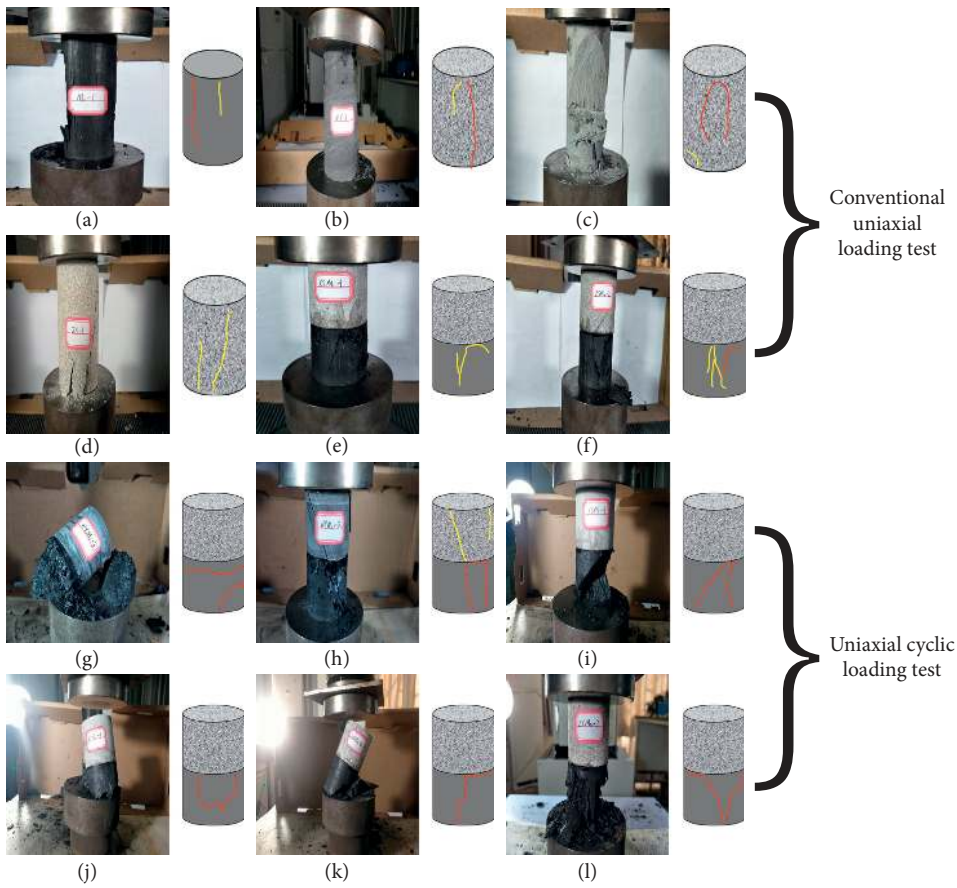

Figure 4: Test results and the failure modes of samples: (a) M1-1, (b) NY-1, (c) XS-1, (d) ZS-1, (e) XSM1-1, (f) ZSM2-2, (g) NYM1-3, (h) NYM1-4, (i) XSM1-3, (j) XSM1-4, (k) ZSM2-6, (l) ZSM2-7 (in the figure, the yellow line indicates the position of the crack after the failure of the sample, and the red line represents the boundary of the spalling area of the sample).

failure characteristics of coal and rock. The stress-strain curves obtained from the loading tests are shown in Figures 5 and 6. The compressive strength, peak strain, and Young's modulus of the samples are listed in Table 2.

The failure characteristics of the samples are shown in Figure 4 in the conventional uniaxial and uniaxial cyclic loading tests. It can be seen that in the conventional uniaxial loading tests, most of the coal and rock samples have a penetrating failure. The failure surface of the coal sample is rough, and the failure surface of the rock sample is smooth. The coal body of coal-rock combinations has the penetrating failure, but the rock body is not substantially damaged. In the uniaxial cyclic loading test, the failure of coal-rock combination samples was the same as that of coal-rock combination samples in the conventional uniaxial loading test. In the test process, debris ejection is found in mudstone, fine sandstone, and coal-rock combination bodies, and there is no debris ejection in medium sandstone samples during loading. In the uniaxial cyclic loading test, a large coal body caves out of the test bench. Compared with the failure of the coal-rock combination in uniaxial cyclic loading tests, when the roof lithology is soft, the roof rock will break with the coal body and produce penetrating cracks. When the roof lithology is hard, the roof rock will not break with the coal body.

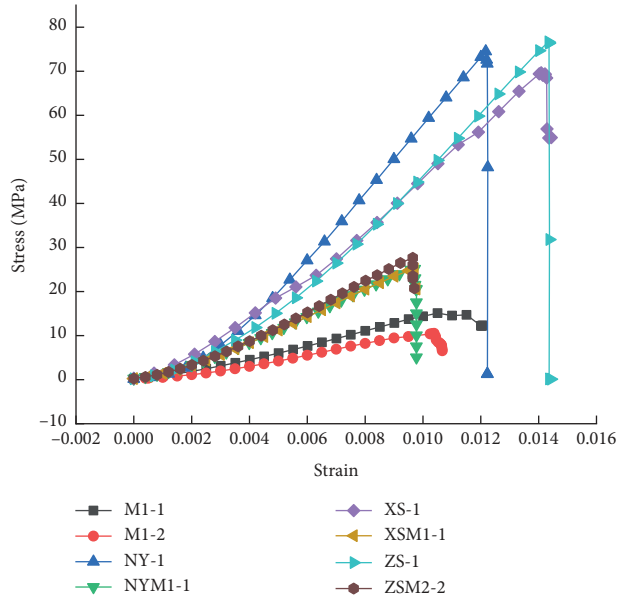

Figure 5: Curves of conventional uniaxial loading test results.

From this analysis, there are a large number of microcracks in the coal and rock samples. The failure of the sample is due to the formation of macrocracks. The microcracks in

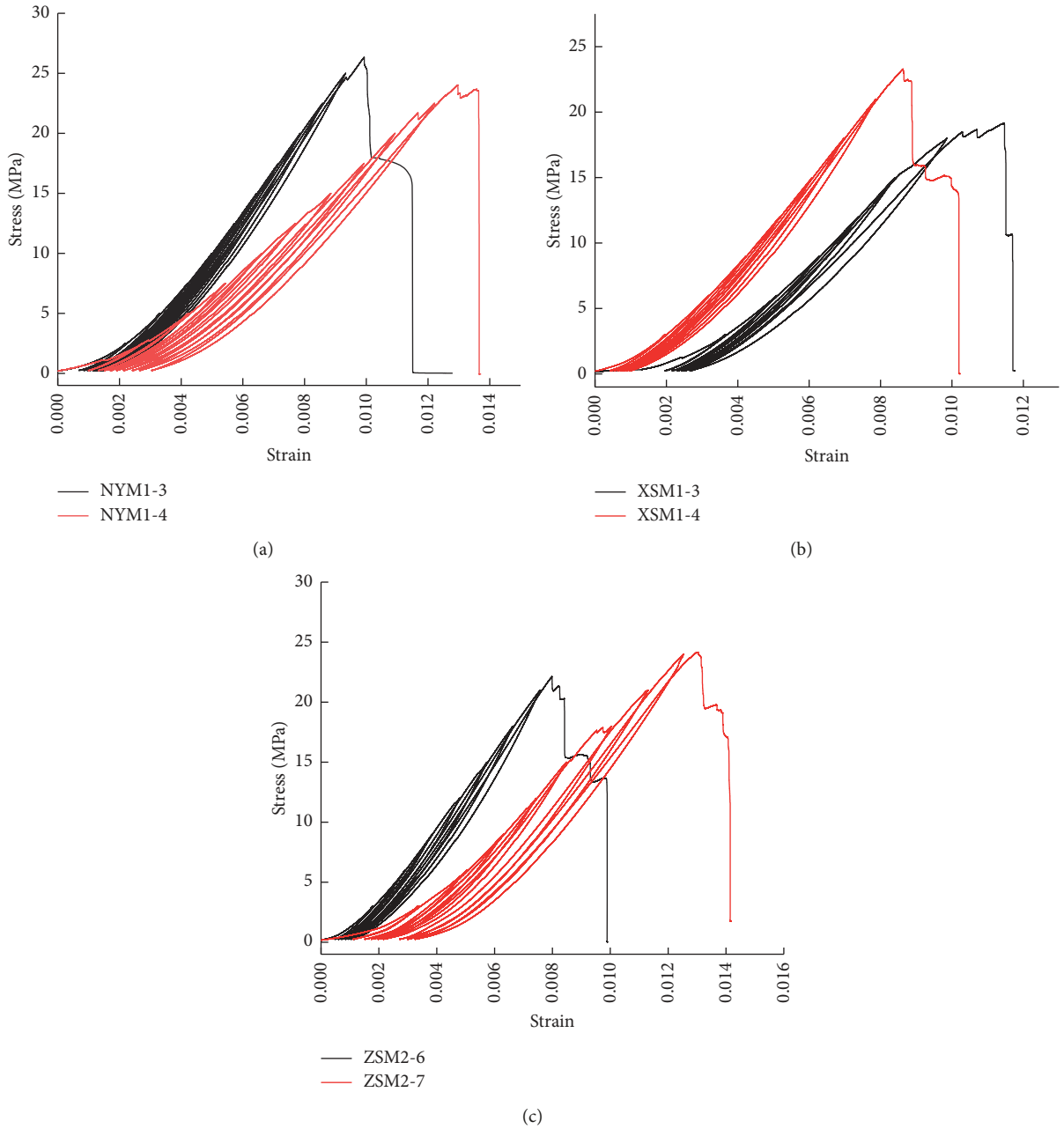

Figure 6: Curves of uniaxial cyclic loading test results: (a) NYM1, (b) XSM1, (c) ZSM2.

Table 2: Test results.

Samples	Compressive strength (MPa)	Axial strain at peak stress (10^{-3})	Young's modulus (GPa)
M1-1	15.3	11.95	1.61
M1-2	11.5	10.67	1.25
NY-1	74.5	12.57	7.52
NYM1-1	26.3	9.71	2.93
NYM1-3	25.32	11.31	—
NYM1-4	22.52	13.52	—
XS-1	69.6	14.09	6.11
XSM1-1	25.2	9.71	2.96
XSM1-3	20.16	11.54	—
XSM1-4	23.31	9.94	—
ZS-1	76.7	14.34	6.79
ZSM2-2	27.7	9.65	3.30
ZSM2-6	22.13	12.72	—
ZSM2-7	24.16	14.19	—

the samples continuously sprout, expand, penetrate, and finally form macrocracks. Then, the macrocracks will cause the failure of samples. At the same time, it is found that there are more microcracks in the coal samples than those in the rock samples. Under the action of external forces, the microcracks in coal bodies expand and penetrate rapidly, which destroys the coal bodies at lower pressure. During the test, the samples will make a slight noise, which is due to the expansion and penetration of microcracks under the action of external forces. The closer the peak intensity is, the more frequent the noise is. This indicates that when the cracks are near the peak strength, a large number of microcracks will expand and penetrate.

Comparing the curves in Figure 5, the elastic and yield stages of rock samples and coal-rock combinations are longer, and the plastic failure stage is less obvious. The stress decreases rapidly after the peak point, and the postpeak curves are very short, showing a sudden brittle failure. Before the failure of the coal samples, there is an obvious plastic failure stage. In this stage, the microcracks further increase and expand, and plastic deformation of the sample occurs. The stress after the peak decreases slowly and then rapidly decreases, showing the characteristics of brittle failure.

Compared with the curves in Figure 6, the postrupture stage of the coal-rock combination curves in the uniaxial cyclic loading test is closely related to the roof lithology. For the combinations with hard roof lithology, the residual strain after the peak is less and the failure of the samples is close to a brittle failure. On the contrary, the combinations with weaker roof lithology have more residual strains after peak, and the samples show obvious progressive failure characteristics.

Comparing the stress-strain curves in Figures 5 and 6, it can be found that the curves of coal-rock combinations have obvious compaction, elastic deformation, and yield stages, and the plastic failure stage is not obvious. After the peak stress, the stress decreases rapidly and the curves behind the peak are very short, showing a sudden brittle fracture. In the uniaxial cyclic loading test, the cyclic curves at the peak have a complete change stage. Unlike the conventional uniaxial loading tests, the cyclic curves at the peak have obvious plastic failure and postrupture stages, with residual stress remaining after the peak and showing progressive failure.

From this analysis, the main reason for the large gap in the failure characteristics of samples lies in the different loading modes. During the conventional uniaxial loading test, the elastic strain of samples cannot be stabilised, and it was characterised by sudden brittle failure and no obvious postrupture stage. In the process of uniaxial cyclic loading, the samples were repeatedly compacted, the elastic deformation decreased, and the elastic strain tended to be stable, showing progressive failure and obvious postrupture stage.

By comparing and analysing the strain at the peak of each sample in Table 2, it can be found that the average axial strain at the peak of coal samples was 0.01131 in the conventional uniaxial loading test, and the axial strains at the peak of rock samples were larger than that of coal sample, which were 0.01257, 0.01409, and 0.01434, respectively. However, the axial strains at the peak value of coal-rock combinations were 0.00971, 0.09971, and 0.00965, which were smaller than those of coal and rock samples. This showed that the deformation degree of coal-rock combinations was lower than that of coal and rock samples under the condition of conventional uniaxial loading tests. In the uniaxial cyclic loading test, the average axial strains at the peak stress of coal-rock combinations were 0.012415, 0.01074, and 0.013455, which were larger than the axial strain at the peak stress of coal-rock combinations in conventional uniaxial loading tests. This showed that the loading method could improve the deformation degree of the samples.

3.2. Compressive Strength and Deformation Characteristics

3.2.1. Compressive Strength. Compressive strength is one of the basic mechanical properties of rock and other materials, and it is also one of the commonly used parameters to judge the strength of samples [44–46]. The stress-strain curves obtained from the loading tests are shown in Figures 6 and 7. The compressive strength, peak strain, and Young's modulus of the samples are listed in Table 2.

By comparing and analysing the test results in Table 2, it was found that the uniaxial compressive strength of three different combinations was 26.3, 25.2, and 27.7 MPa under the conventional uniaxial loading test. Under the uniaxial cyclic loading test, the average compressive strength of the corresponding combinations was 23.8, 21.24, and 23.15 MPa; hence, the compressive strength decreased by 9.05%, 15.71%, and 16.43%, respectively. The uniaxial compressive strength of rock samples measured by the conventional uniaxial loading test was 74.5, 69.2, and 76.7 MPa. Compared with the uniaxial compressive strength of the corresponding coal-rock combinations, the compressive strength of rock in coal-rock combinations was reduced by 64.70%, 63.58%, and 63.89%, respectively. The average uniaxial compressive strength of coal samples was 13.4 MPa. Compared with the uniaxial compressive strength of the coal-rock combination, the compressive strength of coal in a coal-rock combination was increased by 96.27%, 88.06%, and 106.72%, respectively. By analysing the above test results, it can be found that under the cyclic loading, the uniaxial compressive strength of the combinations is greatly reduced, with an average decrease of 64.06%. It shows that the cyclic loading can weaken the strength of the samples.

The results showed that the uniaxial compressive strength of coal-rock combinations measured in the conventional uniaxial loading test was higher than that of coal samples but lower than that of rock samples. The ultimate strength of coal-rock combinations obtained in the uniaxial cyclic loading test was slightly lower than the uniaxial compressive strength of coal-rock combinations. The compressive strength of roof rocks is negatively correlated with the compressive strength of the coal-rock combination itself. Under cyclic loading conditions, the sample is

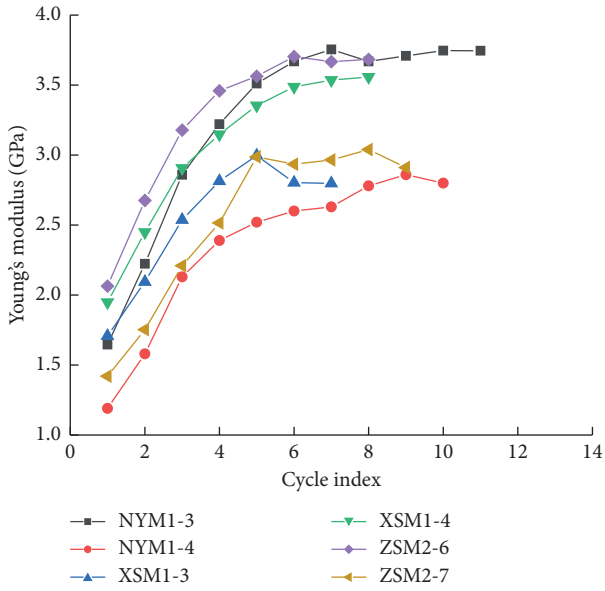

Figure 7: Young's modulus-cycle index curves.

repeatedly compacted, which will weaken its ability to resist deformation and reduce its compressive strength.

From this analysis, the existence of coal in the combination will have a certain impact on the mechanical properties of rock and could weaken its mechanical properties. Moreover, because of the existence of rock, the compressive strength of coal is effectively enhanced, and it does not easily fail. Therefore, it can be considered that the roof rock has a certain protective effect on the coal body.

3.2.2. Young's Modulus. Young's modulus is a physical quantity that describes the elasticity of coal and rock, and it is an important index to judge their degree of elastic deformation [47, 48]. The uniaxial cyclic loading curves were further analysed. Young's modulus of each loading curve of the combinations was calculated by using analysis software. The results are listed in Table 3, and Young's modulus-cycle index curves were obtained by fitting it with the cycle index, as shown in Figure 7. From the figure, we can see that Young's modulus of most samples increased rapidly during U_5-U_6 cycles and then fluctuated within a certain range. In some samples, it even decreased slightly. Fitting Young's modulus of U_5-U_6 cycles before uniaxial cycling loading with the cycle index, it was found that the fitting curve was a logarithmic function ($R^2 \geq 0.95$), which was the same as that of the results of Li's research [49]. However, through further analysis of the data, Young's modulus of the whole cycle was fitted with the cycle index. It was found that most of the fitting curves are quadratic functions downward from the opening, and the correlation coefficients are above 0.95. The fitting results are presented in Table 3, which shows that the fitting curves reflected the variation of Young's modulus of the sample with the cycle index more truthfully.

Therefore, in the early stage of uniaxial cyclic loading, the internal microcracks of the samples develop rapidly and are compacted continuously under the action of external forces. This resulted in the increase in Young's modulus of the samples during the first few cycles. After U_5-U_6 cycles, the internal cracks of the test piece were fully developed and expanded, and the samples reached their elastic limit. Therefore, Young's modulus of the samples does not change significantly, and it fluctuates within a certain range with the cycle index.

Table 3: Fitting results of Young's modulus-cycle index curves.

Specimen number	Fitting equation	Correlation coefficient (R^2)
NYM1-3	$y = -0.0302x^2 + 0.5597x + 1.3014$	0.9563
NYM1-4	$y = -0.0289x^2 + 0.4846x + 0.7955$	0.974
XSM1-3	$y = -0.0634x^2 + 0.6913x + 1.0393$	0.98
XSM1-4	$y = -0.0426x^2 + 0.6059x + 1.4095$	0.997
ZSM2-6	$y = -0.0547x^2 + 0.7059x + 1.4666$	0.9893
ZSM2-7	$y = -0.0422x^2 + 0.6177x + 0.7734$	0.9812

Under the uniaxial cyclic loading condition, it can be found that Young's modulus of the samples after U_5-U_6 cycles is slightly larger than that obtained from the conventional uniaxial loading test. This indicates that cyclic loading can improve the stiffness of the samples and makes it difficult to deform them.

3.3. Law of Energy Evolution

3.3.1. Elastic Energy Density and Dissipative Energy Density. The essence of the deformation and failure of coal and rock is a type of instability phenomenon driven by energy. Deformation and instability of coal and rock are accompanied by energy dissipation and release. Therefore, it is of great significance to study the law of rock and coal energy evolution to explain the mechanical characteristics and failure mechanism of rock and coal under stress [50–55]. Under laboratory conditions, the energy evolution of coal and rock samples can be divided into four processes: energy input, energy accumulation, energy dissipation, and energy release. Among them, energy accumulation and energy dissipation occur almost at the same time. In the process of loading, without considering other energy losses, part of the input energy can cause the elastic deformation of the sample, which accumulates in the form of elastic deformation energy. This part of the energy can be released when unloading. At the same time, microcracks are continuously generated, developed, and penetrated in the sample. The other part of the energy is dissipated in the form of dissipated energy in the process [56]. In this study, the energy evolution law of the combinations in the cyclic loading test is revealed by studying the variation characteristics of the elastic and dissipated energies.

For convenient calculation, the evolution law of the elastic and dissipated energies is studied by calculating the elastic and dissipated energy densities, which were calculated by graphical integration. The elastic and dissipated energies of coal-rock combinations are equal to the elastic and dissipated energy densities multiplied by the sample volume, respectively. Because the sample volume is the same, the

research of energy density can replace the research of energy. The calculation is shown in Figure 8 [30, 31].

According to the calculation method shown in Figure 8 and the calculation formula as follows, the elastic energy density (W_T), dissipated energy density (W_H), and input energy density (W) of each cycle for the coal-rock combination samples were calculated:

$$\begin{aligned} W_T &= \int_{\varepsilon_2}^{\varepsilon_3} \sigma_x d\varepsilon, \\ W &= \int_{\varepsilon_1}^{\varepsilon_3} \sigma \, d\varepsilon, \\ W_H &= W - W_T. \end{aligned} \tag{1}$$

The elastic and dissipated energy densities before the peak of the combination were fitted with the respective cycle index, and the fitting curves shown in Figure 9 were obtained. It can be seen from the figure that the energy density curves of the three coal-rock combinations showed a nonlinear trend, which is similar to the quadratic function curve, and the elastic and dissipated energy densities increased with the increase in cycle index. With the increase in cycle index, the slope of the curve increased and the speed of the energy density also increased. In the process of cycle loading, the elastic energy density curves of the coal-rock combinations were always very close to the energy density curves, while the dissipated energy density curves clearly deviated from the curves. This showed that the cumulative velocity and quantity of elastic energy were higher than the dissipated energy with the increase in cycle index.

The ratios of elastic energy density and dissipated energy density to energy density, respectively, were fitted with the cycle index, and the curves shown in Figure 10 were obtained. It can be seen from the figure that the elastic energy density accounted for almost 80% of the input energy density, which was always in the dominant position, and most of the energy in the input samples was stored in the form of elastic energy. This indicated that more energy was stored in the form of elastic energy in the combination and less energy was released in the form of dissipated energy.

Figure 11 presents the characteristic diagram of cyclic loading and unloading failure. It can be seen from the figure that the higher the cycle index, the more serious the failure of the samples. With the increase in cycle index, the accumulated elastic energy in the coal-rock combinations increased continuously. When these elastic energies were released, it was released in the form of kinetic energy, which aggravated the failure of the samples.

In summary, the higher the ratio of elastic energy stored in the rock samples to the input energy, the more obvious the elasticity and the more the kinetic energy released during failure.

3.3.2. Elastic Energy Index. The elastic energy index refers to the ratio of the accumulated elastic strain energy to the dissipated plastic strain energy in a uniaxial loading test [57, 58]. The elastic energy index (W_{ET}) is calculated by the following formula, and the calculation model is shown in Figure 8:

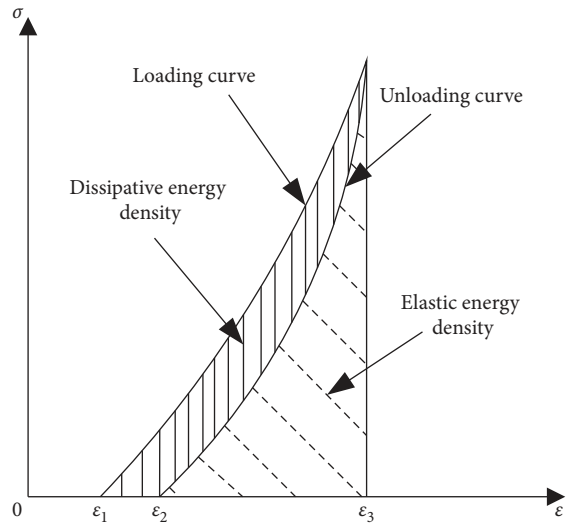

Figure 8: Energy density model.

$$W_{ET} = \frac{W_T}{W_H}. \tag{2}$$

To verify the validity of the previous point of view, the experimental data were further processed. According to the elastic energy density and dissipative energy density, the elastic energy index of each combined cycle is calculated. The curve of elastic energy index is shown in Figure 12. The analysis data showed that the elastic energy index of the combination increased first, then stabilised, and then decreased with the increase in cycle index. The elastic energy index of the first two cycles varied greatly, indicating that cyclic loading could change the kinetic energy released when the sample was damaged. With the increase in cycle index, the elastic energy index of the combinations decreased, but the elastic energy index of the cycle before the samples were destroyed was still much larger than that of the first cycle. The cyclic loading test made the coal-rock combinations store more elastic energy, and they would release more kinetic energy when samples were destroyed. This was a good verification of the above point of view.

4. Discussion

Engineering practice shows that the stress environment of an underground coal mine is complex. The mining stress and original rock stress superimpose on the coal seam and roof rock, which is similar to a cyclic loading condition. Coal mine disasters are mostly generated by the overall structure of coal seam and roof [59–70]. Many coal mine disasters demonstrate that roof-and-floor rock has a loading effect on the failure of the coal seam. For this reason, the deformation and failure characteristics and energy evolution law of coal-rock combinations under a cyclic loading condition were studied experimentally. The experimental results show that

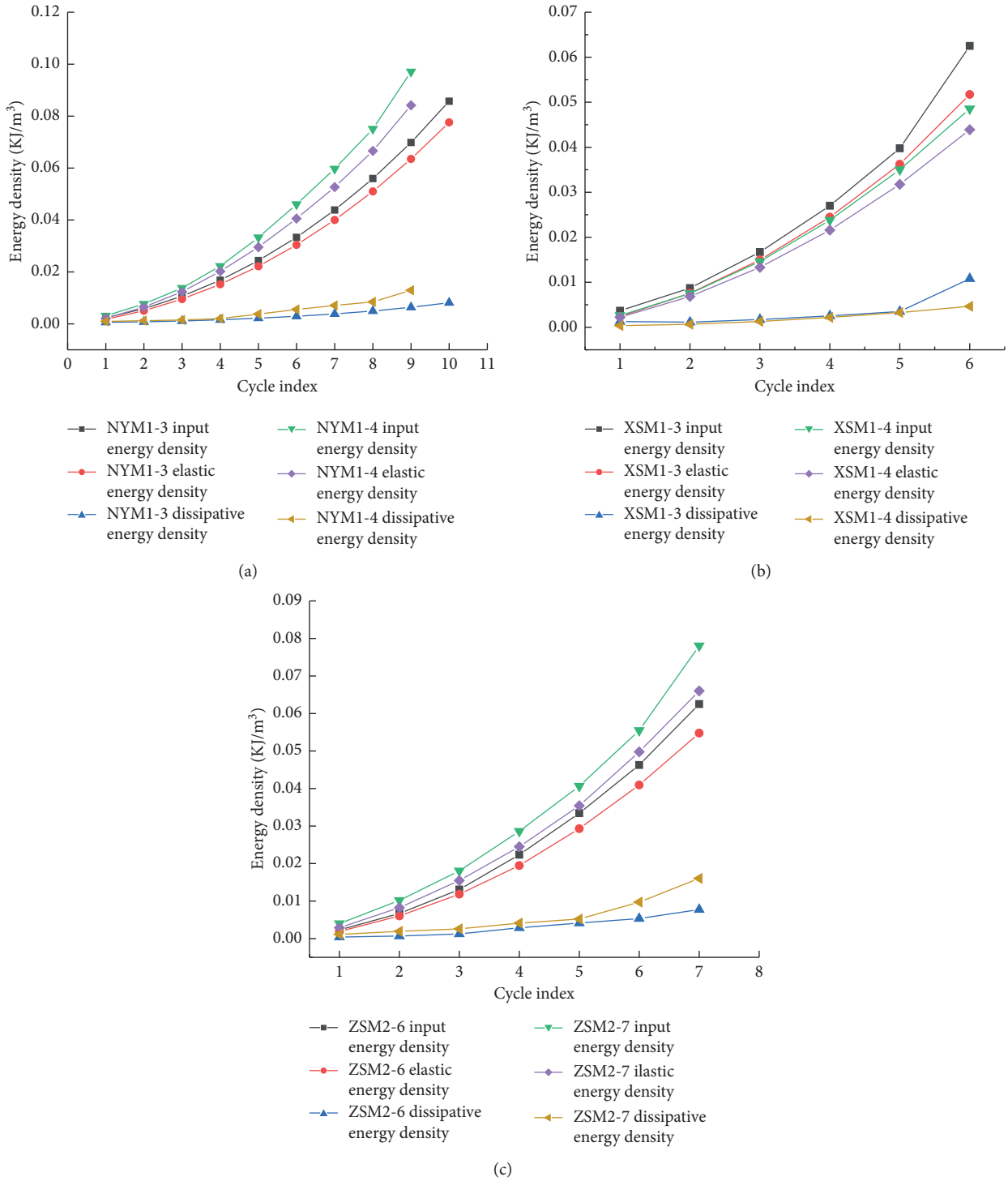

Figure 9: Energy density curves.

the failure modes and mechanical properties of coal-rock combinations under uniaxial cyclic loading are very different from those under uniaxial loading conditions. The failure characteristics of coal-rock combinations are more in line with the actual situation. Under uniaxial cyclic loading, the fitting curves of energy density and cycle index of the coal-rock combination showed a nonlinear growth trend.

In the existing studies, Li et al. [49] carried out uniaxial cyclic loading tests on fractured rock and repeated fatigue tests at the same unloading level. It was found that Young's modulus of the sample was logarithmic to the unloading level. In this study, the relationship between Young's modulus of coal-rock combinations and the cycle index is studied by uniaxial cyclic loading tests. The test results show

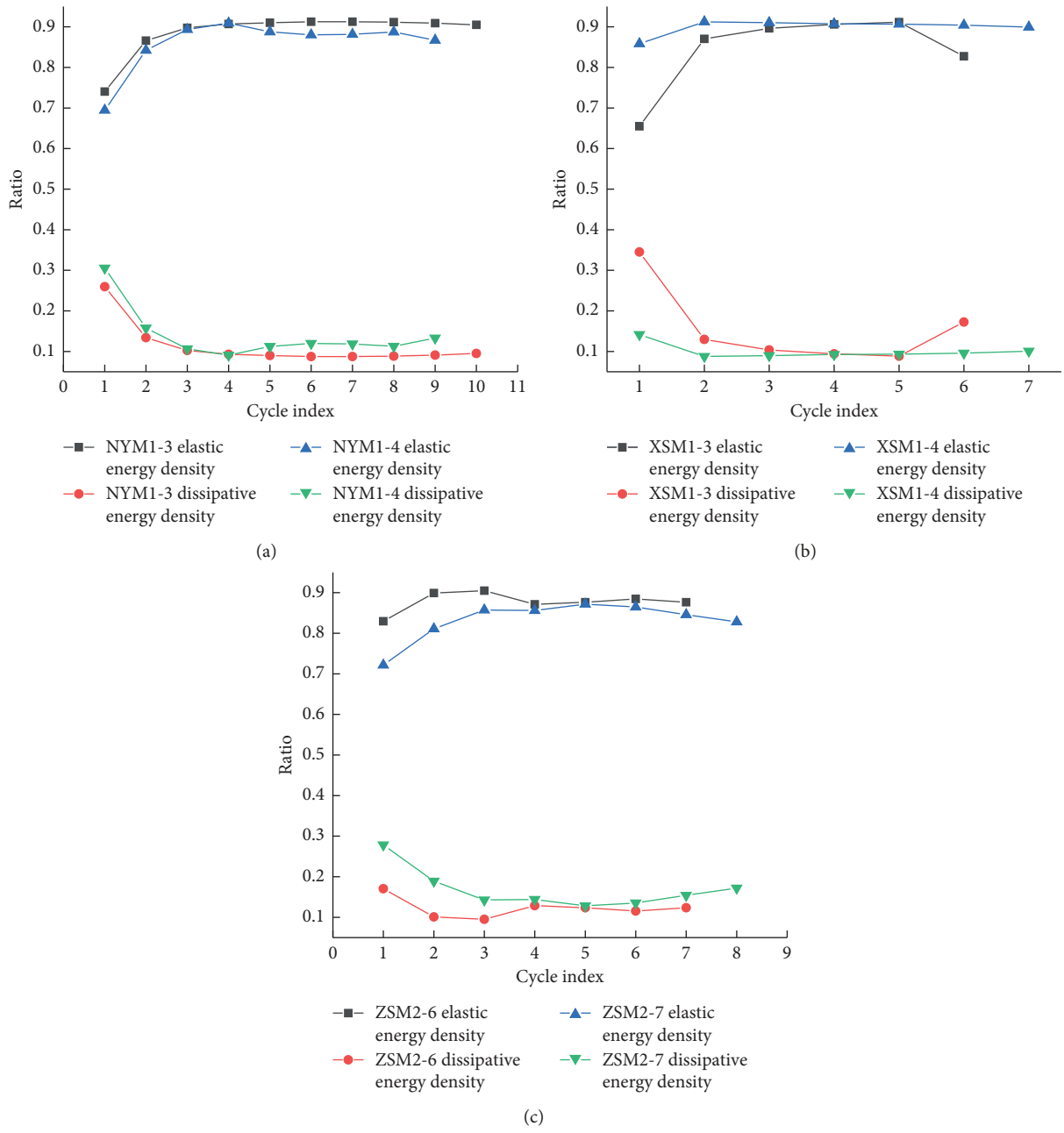

Figure 10: Ratio of elastic energy density and dissipative energy density: (a) NYM1. (b) XSM1. (c) ZSM2.

that Young's modulus of coal-rock combinations has a quadratic function relationship with the cycle index. The fitting curves are shown in Figure 13, and the fitting equation is presented in Table 3. The correlation coefficients were above 0.95, which showed that the fitting curves could reflect the real situation better. The difference between the two test results is due to the differences in the test pieces used. The former uses fractured rock, and the latter uses coal-rock combinations. Another reason may be the difference of loading methods. The former is based on the fatigue test, and this paper is only obtained by the uniaxial cyclic loading test. Yang et al. [56] carried out conventional uniaxial and uniaxial cyclic loading tests on coal samples, rock samples, and coal-rock combinations. It was found that the input energy, elastic energy, and dissipation energy of the combinations in the prepeak stage had a nonlinear relationship with the axial stress. Furthermore, when the yield stage was reached, there was a sudden change point of the dissipated energy, and then, the ratio of dissipated energy increased more. In this study, the input, elastic, and dissipated energies were fitted with the cycle index. It was found that the curves also showed a nonlinear growth, which validated the above research. The difference is that, as can be seen from Figure 9, the ratio of dissipated energy of most samples decreased first and then increased and the ratio of dissipated energy increased more in the last 1-2 cycles.

(a) (b) (c) (d)

Figure 11: Failure characteristics of cyclic loading of samples. (a) Four cycles. (b) Seven cycles. (c) Eight cycles. (d) Ten cycles.

Based on the experimental study of coal samples, rock samples, and coal-rock combinations, the failure modes, strength, and deformation characteristics of coal-rock combinations under two uniaxial loading conditions were obtained. The energy evolution law of coal-rock combinations under cyclic loading conditions was studied and analysed. The variation law of the input, elastic, and dissipated energies with the cycle index was obtained, and the fitting equations were also obtained. It well reveals the influence of cycle index on the law of energy evolution. It is of great significance to study the failure modes, deformation characteristics, and energy evolution of coal and rock structures in situ, and this work is expected to provide parameter support for the design and evaluation of underground engineering projects related to coal mines.

In this study, the deformation, failure, and energy evolution of coal-rock combinations were systematically studied, and some valuable conclusions were obtained. Although the elastic energy index of coal-rock combinations was calculated, its threshold value was different from that of coal samples. At present, the research cannot obtain this important numerical value. In the future work, we also need to carry out a large number of indoor tests to study the effects of combination mode and loading methods on the failure mode, mechanical properties, and energy evolution of coal-rock combinations. Combined with the actual situation of the site, we need to present a more reasonable method and a threshold for evaluating the coal burst tendency of coal seams. By this, it can provide a more reliable basis for the evaluation of field engineering coal

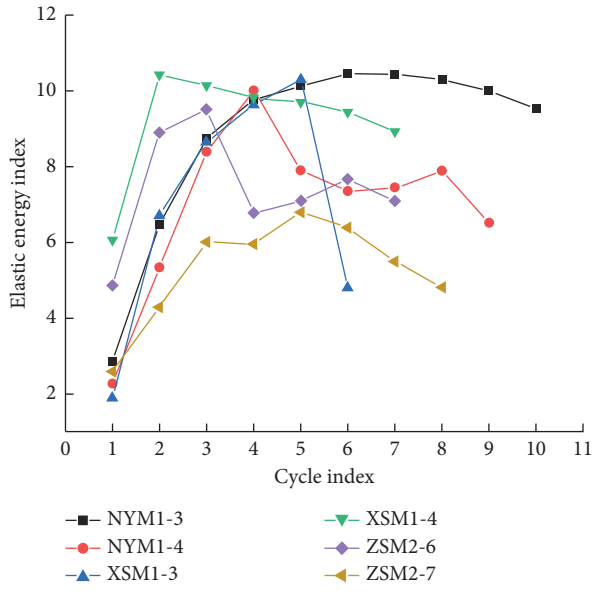

Figure 12: Elastic energy exponential curves.

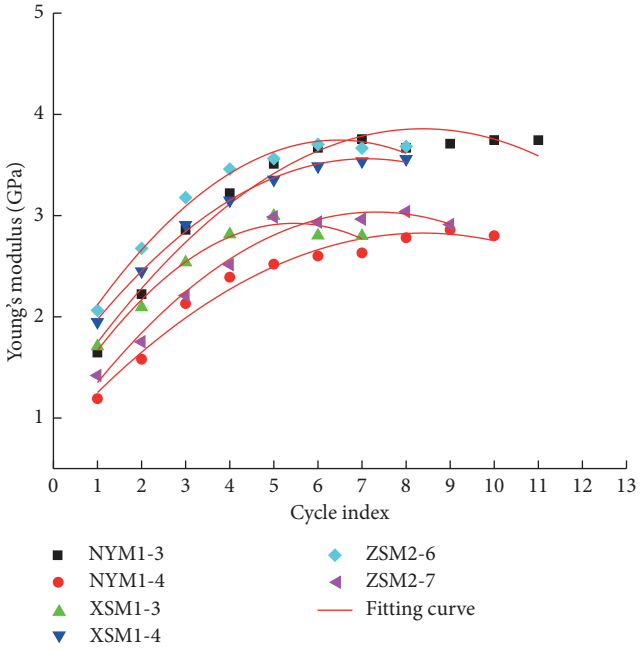

Figure 13: Fitting curves of Young's modulus-cycle index.

burst tendency so that the experimental research can better serve the field.

5. Conclusion

In this study, the effects of loading mode, cycle index, and rock properties on the mechanical properties of coal-rock combinations were systematically analysed through conventional uniaxial and uniaxial cyclic loading tests.

(1) There were mainly three types of failure modes during the tests: shear slip, tensile splitting, and fracture. Under the conventional uniaxial loading condition, the main failure mode of the samples was fracture failure, and a few of them had tensile splitting failure. Under the uniaxial cyclic loading test condition, the main failure mode of the samples was shear slip failure. All the coal sections in coal-rock combinations failed, whereas most rock sections remained intact.

(2) The compressive strength of a coal-rock combination was larger than that of coal and much smaller than that of rock. Under the conventional uniaxial loading condition, the uniaxial compressive strength of the coal-rock combinations was approximately 97.02% larger than that of the coal section and approximately 60% of that of the rock section. Under the cyclic loading condition, both the maximum deformation before failure and Young's modulus of coal-rock combinations were larger than those under the conventional uniaxial loading condition, and the latter increased logarithmically with the cycle index.

(3) The elastic energy stored in coal-rock combinations played a dominant role in the distribution of all input energy, accounting for more than 80% of it. Most energy was released in the form of kinetic energy during the failure process, which aggravated the damage degree. With the increase in cycle index, both the elastic energy stored in the sample and the dissipated energy increased in a quadratic function, and the failure process became more intense.

Data Availability

The data used to support the findings of this study are included within the article.

Conflicts of Interest

The authors declare no conflicts of interest.

Acknowledgments

This research was funded by the National Key R&D Program of China (No. 2018YFC0604703), National Natural Science Foundation of China (Nos. 51804181, 51874190, and 51574154), Major Program of Shandong Province Natural Science Foundation (No. ZR2018ZA0603), Shandong Province Natural Science Fund (No. ZR2018QEE002), Key R&D Program of Shandong Province (No. 2019GSF111020), Open Fund of State Key Laboratory of Water Resource Protection and Utilization in Coal Mining (No. GJNY-18-73.5), Tai'shan Scholar Engineering Construction Fund of Shandong Province of China (No. ts201511026), and SDUST Graduate Student Technology Innovation Project (No. SDKDYC190234).

References

[1] Z. L. Li, X. Q. He, L. M. Dou, D.-Z. Song, G.-F. Wang, and X.-L. Xu, "Investigating the mechanism and prevention of

coal mine dynamic disasters by using dynamic cyclic loading tests," *Safety Science*, vol. 115, pp. 215–228, 2019.

[2] Y. C. Yin, T. B. Zhao, Y. B. Zhang et al., "An innovative method for placement of gangue backfilling material in steep underground coal mines," *Minerals–Basel*, vol. 9, no. 2, p. 107, 2019.

[3] Y. L. Tan, D. Y. Fan, X. S. Liu, S. Song, X. F. Li, and H. L. Wang, "Numerical investigation on failure evolution of surrounding rock for super-large section chamber group in deep coal mine," *Energy Science & Engineering*, pp. 1–23, 2019.

[4] H. M. Yang, G. C. Wen, Q. T. Hu, Y. Y. Li, and L. C. Dai, "Experimental investigation on influence factors of acoustic emission activity in coal failure process," *Energies*, vol. 11, no. 6, p. 1414, 2018.

[5] J. G. Ning, X. S. Liu, J. Tan, Q. H. Gu, Y. L. Tan, and J. Wang, "Control mechanisms and design for a "coal-backfill-gangue" support system for coal mine gob-side entry retaining," *International Journal of Oil, Gas and Coal Technology*, vol. 18, no. 3-4, pp. 444–466, 2018.

[6] S. J. Chen, X. Qu, D. W. Yin, X. Q. Liu, H. F. Ma, and H. Y. Wang, "Investigation lateral deformation and failure characteristics of strip coal pillar in deep mining," *Geomechanics and Engineering*, vol. 14, no. 5, pp. 421–428, 2018.

[7] Y. L. Tan, Q. Ma, Z. H. Zhao et al., "Cooperative bearing behaviors of roadside support and surrounding rocks along gob-side," *Geomechanics and Engineering*, vol. 18, no. 4, pp. 439–448, 2019.

[8] Y. Y. Li, S. C. Zhang, and X. Zhang, "Classification and fractal characteristics of coal rock fragments under uniaxial cyclic loading conditions," *Journal of Geosciences*, vol. 11, no. 9, p. 201, 2018.

[9] J. Q. Xiao, D. X. Ding, G. Xu et al., "Deformation characteristics of rock under constant amplitude cyclic loading," *Journal of Central South University*, vol. 41, pp. 685–691, 2010.

[10] Y. L. Wei, C. H. Yang, Y. T. Guo, W. Liu, L. Wang, and S. Heng, "Experimental investigation on deformation and fracture characteristics of brittle shale with natural cracks under uniaxial cyclic loading," *Rock and Soil Mechanics*, vol. 36, pp. 1649–1658, 2015.

[11] Y. J. Yang, L. Y. Xing, H. Q. Duan, L. Deng, and Y.-C. Xue, "Fatigue damage evolution of coal under cyclic loading," *Arabian Journal of Geosciences*, vol. 11, no. 18, p. 560, 2018.

[12] Y. J. Yang, H. Q. Duan, L. Y. Xing, S. Ning, and J. Lv, "Fatigue characteristics of limestone under triaxial compression with cyclic loading," *Advances in Civil Engineering*, vol. 2018, Article ID 8681529, 12 pages, 2018.

[13] Y. J. Yang, H. Q. Duan, L. Y. Xing, and L. Deng, "Fatigue characteristics of coal specimens under cyclic uniaxial loading," *Geotechnical Testing Journal*, vol. 42, no. 2, pp. 331–346, 2019.

[14] S. Q. Yang, P. G. Ranjith, Y.-H. Huang et al., "Experimental investigation on mechanical damage characteristics of sandstone under triaxial cyclic loading," *Geophysical Journal International*, vol. 201, no. 2, pp. 662–682, 2015.

[15] J. Liu, J. L. Li, Y. D. Zhang et al., "Analysis of energy characteristics and deformation parameters of rock mass under cyclic loading," *Chinese Journal of Rock Mechanics and Engineering*, vol. 29, pp. 3505–3513, 2010.

[16] X. L. Yang, J. Cao, X. Y. Cheng et al., "Mechanical response characteristics and permeability evolution of coal samples under cyclic loading," *Energy Science & Engineering*, vol. 7, no. 5, pp. 1588–1604, 2019.

[17] H. F. Deng, Y. Hu, J. L. Li et al., "The evolution of sandstone energy dissipation under cyclic loading and unloading," *Chinese Journal of Rock Mechanics and Engineering*, vol. 35, pp. 2869–2875, 2016.

[18] Y. Zhang, J. Xu, H. W. Yang, and J. Wang, "Effect of confining pressure on evolution law of hysteresis loop of sandstone under cyclic loading," *Chinese Journal of Rock Mechanics and Engineering*, vol. 30, pp. 320–326, 2011.

[19] X. B. Yang, Y. P. Qin, and F. Ye, "Damage constitutive relation of sandstone considering residual stress," *Journal of China Coal Society*, vol. 40, pp. 2807–2811, 2015.

[20] P. Xu, J. B. Zhou, J. Huang et al., "Damage evolution and strain energy characteristic of marble under triaxial cyclic compression," *Journal of Yangtze River Scientific Research Institute*, 2019.

[21] E. Liu, S. He, X. Xue, and J. Xu, "Dynamic properties of intact rock samples subjected to cyclic loading under confining pressure conditions," *Rock Mechanics and Rock Engineering*, vol. 44, no. 5, pp. 629–634, 2011.

[22] Z. H. Zhao, W. M. Wang, C. Q. Dai, and J. X. Yan, "Failure characteristics of three-body model composed of rock and coal with different strength and stiffness," *Transactions of Nonferrous Metals Society of China*, vol. 24, no. 5, pp. 1538–1546, 2014.

[23] X. S. Liu, Y. L. Tan, J. G. Ning, Y. W. Lu, and Q. H. Gu, "Mechanical properties and damage constitutive model of coal in coal-rock combined body," *International Journal of Rock Mechanics and Mining Sciences*, vol. 110, pp. 140–150, 2018.

[24] Y. L. Tan, X. S. Liu, B. Shen, J. G. Ning, and Q. H. Gu, "New approaches to testing and evaluating the impact capability of coal seam with hard roof and/or floor in coal mines," *Geomechanics and Engineering*, vol. 14, pp. 367–376, 2018.

[25] S. J. Chen, D. W. Yin, B. L. Zhang, H. F. Ma, and X. Q. Liu, "Mechanical characteristics and progressive failure mechanism of roof–coal pillar structure," *Chinese Journal of Rock Mechanics and Engineering*, vol. 36, no. 7, pp. 1588–1598, 2017.

[26] Z. T. Zhang, J. F. Liu, L. Wang, H.-T. Yang, and J.-P. Zuo, "Effects of combination mode on mechanical properties and failure characteristics of the coal–rock combinations," *Journal of China Coal Society*, vol. 37, no. 10, pp. 1677–1681, 2012.

[27] H. Q. Song, J. P. Zuo, Y. Chen et al., "Post–peak stress–strain relationship model and brittle characteristics of coal–rock combined body," *Journal of Mining and Safety Engineering*, vol. 35, pp. 1063–1070, 2018.

[28] J. P. Zuo, H. Q. Song, Y. Chen, and Y. H. Li, "Post-peak progressive failure characteristics and nonlinear model of coal–rock combined body," *Journal of China Coal Society*, vol. 43, no. 12, pp. 3265–3272, 2018.

[29] Z. H. Zhu, T. Feng, F. Q. Gong et al., "Experimental research of mechanical properties on grading cycle loading–unloading behavior of coal–rock combination bodies at different stress levels," *Journal of Central South University*, vol. 47, pp. 2469–2475, 2016.

[30] F. Gong, J. Yan, X. Li, and S. Luo, "A peak-strength strain energy storage index for rock burst proneness of rock materials," *International Journal of Rock Mechanics and Mining Sciences*, vol. 117, pp. 76–89, 2019.

[31] L. Z. Tang and W. X. Wang, "A new index of rock burst tendency," *Chinese Journal of Rock Mechanics and Engineering*, vol. 21, pp. 874–878, 2002.

[32] D. Y. Fan, X. S. Liu, Y. L. Tan, L. Yan, S. Song, and J. G. Ning, "An innovative approach for gob-side entry retaining in deep coal mines: a case study," *Energy Science & Engineering*, pp. 1–15, 2019.

[33] M. Ismael and H. Konietzky, "Constitutive model for inherent anisotropic rocks: ubiquitous joint model based on the Hoek-Brown failure criterion," *Computers and Geotechnics*, vol. 105, pp. 99–109, 2019.

[34] X. S. Liu, J. G. Ning, Y. L. Tan, Q. Xu, and D. Y. Fan, "Coordinated supporting method of gob-side entry retaining in coal mines and a case study with hard roof," *Geomechanics and Engineering*, vol. 15, no. 6, pp. 1173–1182, 2018.

[35] X. S. Liu, Q. H. Gu, Y. L. Tan, J. G. Ning, and Z. C. Jia, "Mechanical characteristics and failure prediction of cement mortar with a sandwich structure," *Minerals*, vol. 9, no. 3, p. 143, 2019.

[36] F. Meng, L. N. Y. Wong, H. Zhou, J. Yu, and G. Cheng, "Shear rate effects on the post-peak shear behaviour and acoustic emission characteristics of artificially split granite joints," *Rock Mechanics and Rock Engineering*, vol. 52, no. 7, pp. 2155–2174, 2019.

[37] S. F. Liu, Z. J. Wan, J. C. Wang, S.-F. Lu, and T.-H. Li, "Subloading surface model and experimental study of coal failure under cyclic loading," *Advances in Materials Science and Engineering*, vol. 2019, Article ID 9841297, 13 pages, 2019.

[38] M. Q. You and A. Z. Hua, "Fracture of rock specimen and decrement of bearing capacity in uniaxial compression," *Chinese Journal of Rock Mechanics and Engineering*, vol. 17, pp. 292–296, 1998.

[39] L. S. Tang, H. T. Sang, J. Song, Z. G. Luo, and Y.-L. Sun, "Mechanical model for failure modes of rock and soil under compression," *Transactions of Nonferrous Metals Society of China*, vol. 26, no. 10, pp. 2711–2723, 2016.

[40] S. J. Niu, H. W. Jing, and J. Q. Liang, "Experimental study of failure mode of sandstone under different loading paths," *Chinese Journal of Rock Mechanics and Engineering*, vol. 30, pp. 966–3974, 2011.

[41] H. P. Xie, R. D. Peng, and Y. Ju, "Energy dissipation analysis of rock deformation and failure," *Chinese Journal of Rock Mechanics and Engineering*, vol. 23, pp. 3565–3570, 2004.

[42] C. Fan, D. Elsworth, S. Li, L. Zhou, Z. Yang, and Y. Song, "Thermo-hydro-mechanical-chemical couplings controlling CH_4 production and CO_2 sequestration in enhanced coalbed methane recovery," *Energy*, vol. 173, pp. 1054–1077, 2019.

[43] K. Fang, T. Zhao, Y. Zhang, Y. Qiu, and J. Zhou, "Rock cone penetration test under lateral confining pressure," *International Journal of Rock Mechanics and Mining Sciences*, vol. 119, pp. 149–155, 2019.

[44] E. S. P. Fortes, A. F. Guilherme, and S. Fernando, "Relationship between the compressive strength of concrete masonry and the compressive strength of concrete masonry units," *Journal of Materials in Civil Engineering*, vol. 27, no. 9, Article ID 04014238, 2015.

[45] C. Gaedicke, A. Torres, K. C. T. Huynh, and A. Marines, "A method to correlate splitting tensile strength and compressive strength of pervious concrete cylinders and cores," *Construction and Building Materials*, vol. 125, pp. 271–278, 2016.

[46] T. B. Zhao, S. Q. Ma, and Y. Z. Zhang, "Ground control monitoring in backfilled strip mining under the metropolitan district: case study," *International Journal of Geomechanics*, vol. 18, no. 7, Article ID 05018003, 2018.

[47] Z. Tao, Y. Wang, C. Zhu, H. Xu, G. Li, and M. He, "Mechanical evolution of constant resistance and large deformation anchor cables and their application in landslide monitoring," *Bulletin of Engineering Geology and the Environment*, vol. 78, no. 7, pp. 4787–4803, 2019.

[48] L. Y. Xing, Y. J. Yang, J. K. Lv et al., "Roadside support schemes numerical simulation and field monitoring of gob-side entry retaining in soft floor and hard roof," *AER-Advances in Engineering Research*, vol. 76, pp. 109–114, 2018.

[49] T. Li, X. Pei, D. Wang, R. Huang, and H. Tang, "Nonlinear behavior and damage model for fractured rock under cyclic loading based on energy dissipation principle," *Engineering Fracture Mechanics*, vol. 206, pp. 330–341, 2019.

[50] W. Y. Guo, Y. L. Tan, F. H. Yu et al., "Mechanical behavior of rock–coal–rock specimens with different coal thicknesses," *Geomechanics and Engineering*, vol. 15, no. 4, pp. 1017–1027, 2018.

[51] C. Cui, S. Jiang, K. Wang et al., "Effects of ionic liquid concentration on coal low temperature oxidation," *Energy Science & Engineering*, vol. 7, no. 5, pp. 2165–2179, 2019.

[52] G. Wang, C. H. Jiang, J. N. Shen, D. Y. Han, and X. J. Qin, "Deformation and water transport behaviors study of heterogenous coal using CT-based 3D simulation," *International Journal of Coal Geology*, vol. 211, Article ID 103204, 2019.

[53] B. Kong, E. Y. Wang, Z. H. Li, and W. Lu, "Study on the feature of electromagnetic radiation under coal oxidation and temperature rise based on multi-fractal theory," *Fractals*, vol. 27, no. 3, Article ID 1950038, 2019.

[54] M. Li, J. Zhang, N. Zhou, and Y. Huang, "Effect of particle size on the energy evolution of crushed waste rock in coal mines," *Rock Mechanics and Rock Engineering*, vol. 50, no. 5, pp. 1347–1354, 2017.

[55] Y. L. Tan, Q. H. Gu, J. G. Ning, X. S. Liu, Z. C. Jia, and D. M. Huang, "Uniaxial compression behavior of cement mortar and its damage-constitutive model based on energy theory," *Materials*, vol. 12, no. 8, p. 1309, 2019.

[56] L. Yang, F. Q. Gao, X. X. Wang et al., "Study on energy evolution law and failure mechanism of coal–rock combined specimen," *Journal of China Coal Society*, 2019.

[57] J. Ning, J. Wang, J. Jiang, S. Hu, L. Jiang, and X. Liu, "Estimation of crack initiation and propagation thresholds of confined brittle coal specimens based on energy dissipation theory," *Rock Mechanics and Rock Engineering*, vol. 51, no. 1, pp. 119–134, 2018.

[58] N. Wang, Y. Q. Xu, D. Y. Zhu, N. Wang, and B. Yu, "Acoustic emission and failure modes for coal-rock structure under different loading rates," *Advances in Civil Engineering*, vol. 2018, Article ID 9391780, 11 pages, 2018.

[59] B. Y. Jiang, S. T. Gu, L. G. Wang, G.-C. Zhang, and W.-S. Li, "Strainburst process of marble in tunnel–excavation–induced stress path considering intermediate principal stress," *Journal of Central South University*, vol. 26, no. 4, pp. 984–999, 2019.

[60] D. Y. Fan, X. S. Liu, Y. L. Tan et al., "Roof cutting parameters design for gob–side entry in deep coal mine: a case study," *Energies*, vol. 12, p. 2032, 2019.

[61] G. C. Zhang, Z. J. Wen, S. J. Liang et al., "Ground response of a gob–side entry in a longwall panel extracting 17 m–thick coal seam: a case study," *Rock Mechanics and Rock Engineering*, pp. 1–20, 2019.

[62] J. H. Zhao, N. Jiang, L. M. Yin, and L. Y. Bai, "The effects of mining subsidence and drainage improvements on a waterlogged area," *Bulletin of Engineering Geology and the Environment*, vol. 78, pp. 3815–3831, 2019.

[63] Q. Ma, Y. L. Tan, Z. H. Zhao, Q. Xu, J. Wang, and K. Ding, "Roadside support schemes numerical simulation and field monitoring of gob-side entry retaining in soft floor and hard roof," *Arabian Journal of Geosciences*, vol. 11, no. 563, 2018.

[64] C. Fan, D. Elsworth, S. Li et al., "Modelling and optimization of enhanced coalbed methane recovery using CO_2/N_2 mixtures," *Fuel*, vol. 253, pp. 1114–1129, 2019.

[65] Q. G. Zhang, X. Y. Fan, Y. C. Liang et al., "Mechanical behavior and permeability evolution of reconstituted coal samples under various unloading confining pressures—implications for wellbore stability analysis," *Energies*, vol. 10, no. 3, p. 292, 2017.

[66] M. P. Kuz'min, L. M. Larionov, V. V. Kondratiev, M. Y. Kuz'mina, V. G. Grigoriev, and A. S. Kuz'mina, "Use of the burnt rock of coal deposits slag heaps in the concrete products manufacturing," *Construction and Building Materials*, vol. 179, pp. 117–124, 2018.

[67] G. Wang, J. Shen, S. Liu, C. H. Jiang, and X. J. Qin, "Three-dimensional modeling and analysis of macro-pore structure of coal using combined X-ray CT imaging and fractal theory," *International Journal of Rock Mechanics and Mining Sciences*, vol. 123, Article ID 104082, 2019.

[68] G. Wang, X. J. Qin, J. N. Shen, Z. Y. Zhang, D. Y. Han, and C. H. Jiang, "Quantitative analysis of microscopic structure and gas seepage characteristics of low-rank coal based on CT three-dimensional reconstruction of CT images and fractal theory," *Fuel*, vol. 256, Article ID 115900, 2019.

[69] X. S. Liu, J. G. Ning, Y. L. Tan, and Q. H. Gu, "Damage constitutive model based on energy dissipation for intact rock subjected to cyclic loading," *International Journal of Rock Mechanics and Mining Sciences*, vol. 85, pp. 27–32, 2016.

[70] A. İ. Karayiğita, M. Mastalerzb, R. G. Oskay, and İ. Buzkan, "Bituminous coal seams from underground mines in the Zonguldak Basin (NW Turkey): insights from mineralogy, coal petrography, rock-eval pyrolysis, and meso-and micro-porosity," *International Journal of Coal Geology*, vol. 199, pp. 91–112, 2018.